



UNIVERSITÀ
DEGLI STUDI
FIRENZE

FLORE

Repository istituzionale dell'Università degli Studi di Firenze

Selective HCN1 block as a strategy to control oxaliplatin-induced neuropathy

Questa è la Versione finale referata (Post print/Accepted manuscript) della seguente pubblicazione:

Original Citation:

Selective HCN1 block as a strategy to control oxaliplatin-induced neuropathy / Resta, F.*; Micheli, L.; Laurino, A.; Spinelli, V.; Mello, T.; Sartiani, L.; Di Cesare Mannelli, L.; Cerbai, E.; Ghelardini, C.; Romanelli, M.N.; Mannaioni, G.; Masi, A.. - In: NEUROPHARMACOLOGY. - ISSN 0028-3908. - ELETTRONICO. - 131:(2018), pp. 403-413. [10.1016/j.neuropharm.2018.01.014]

Availability:

This version is available at: 2158/1112380 since: 2018-02-20T10:36:35Z

Published version:

DOI: 10.1016/j.neuropharm.2018.01.014

Terms of use:

Open Access

La pubblicazione è resa disponibile sotto le norme e i termini della licenza di deposito, secondo quanto stabilito dalla Policy per l'accesso aperto dell'Università degli Studi di Firenze (<https://www.sba.unifi.it/upload/policy-oa-2016-1.pdf>)

Publisher copyright claim:

(Article begins on next page)



Selective HCN1 block as a strategy to control oxaliplatin-induced neuropathy

F. Resta ^{a,*}, L. Micheli ^a, A. Laurino ^a, V. Spinelli ^a, T. Mello ^c, L. Sartiani ^a,
L. Di Cesare Mannelli ^a, E. Cerbai ^a, C. Ghelardini ^a, M.N. Romanelli ^b, G. Mannaioni ^{a,1},
A. Masi ^{a,1}

^a Department of Neuroscience, Psychology, Drug Research and Child Health - NEUROFARBA - Pharmacology and Toxicology Section, University of Florence, Florence, Italy

^b Department of Neuroscience, Psychology, Drug Research and Child Health, Section of Pharmaceutical and Nutritional Sciences, University of Florence, via Ugo Schiff 6, Sesto Fiorentino, Italy

^c Clinical Gastroenterology Laboratory, Department of Experimental and Clinical Biomedical Sciences, "Mario Serio" University of Florence, Florence, Italy

ARTICLE INFO

Article history:

Received 28 August 2017

Received in revised form

27 December 2017

Accepted 9 January 2018

Available online 12 January 2018

Keywords:

HCN channels

HCN1

Ih current

Oxaliplatin

Neuropathic pain

ABSTRACT

Chemotherapy-Induced Peripheral Neuropathy (CIPN) is the most frequent adverse effect of pharmacological cancer treatments. The occurrence of neuropathy prevents the administration of fully-effective drug regimen, affects negatively the quality of life of patients, and may lead to therapy discontinuation. CIPN is currently treated with anticonvulsants, antidepressants, opioids and non-opioid analgesics, all of which are flawed by insufficient anti-hyperalgesic efficacy or addictive potential. Understandably, developing new drugs targeting CIPN-specific pathogenic mechanisms would dramatically improve efficacy and tolerability of anti-neuropathic therapies. Neuropathies are associated to aberrant excitability of DRG neurons due to the alteration in the expression or function of a variety of ion channels. In this regard, Hyperpolarization-activated Cyclic Nucleotide-gated (HCN) channels are overexpressed in inflammatory and neuropathic pain states, and HCN blockers have been shown to reduce neuronal excitability and to ameliorate painful states in animal models. However, HCN channels are critical in cardiac action potential, and HCN blockers used so far in pre-clinical models do not discriminate between cardiac and non-cardiac HCN isoforms. In this work, we show an HCN current gain of function in DRG neurons from oxaliplatin-treated rats. Biochemically, we observed a downregulation of HCN2 expression and an upregulation of the HCN regulatory beta-subunit MirP1. Finally, we report the efficacy of the selective HCN1 inhibitor MEL57A in reducing hyperalgesia and allodynia in oxaliplatin-treated rats without cardiac effects. In conclusion, this study strengthens the evidence for a disease-specific role of HCN1 in CIPN, and proposes HCN1-selective inhibitors as new-generation pain medications with the desired efficacy and safety profile.

© 2018 Elsevier Ltd. All rights reserved.

1. Introduction

1.1. Clinical aspects of CIPN

Chemotherapy-induced peripheral neuropathy (CIPN) is a progressive, long-lasting condition characterized by numbness, dysesthesia, hyperalgesia and allodynia (Addington and Freimer, 2016;

Avan et al., 2015). It is estimated that up to 90% of all cancer patients receiving chemotherapy will be affected by CIPN at various severity levels (Bokhari and Sawatzky, 2009). Pain intensity in patients experiencing CIPN is distressing and debilitating and could lead to treatment discontinuation with obvious consequences on clinical outcome (Kim et al., 2015). Due to the lack of specific therapies, CIPN is treated with the same therapeutic approaches employed in other chronic pain states. First-line treatments include voltage-gated calcium channel alpha-2-delta blockers, tricyclic antidepressants, selective serotonin and norepinephrine reuptake inhibitors and local anesthetics. Opioid analgesics represent second-line therapies, while third-line therapies include other

* Corresponding author.

E-mail address: francesco.resta@unifi.it (F. Resta).

¹ Equal contribution.

antidepressant medications, membrane stabilizers, NMDA receptor antagonists, and topical agents (Kim et al., 2015). These classes of drugs often have severe side effects when used chronically. Moreover, none of these drugs is fully effective in the prevention or treatment of CIPN (Cavaletti, 2014; Roberts et al., 1997). The inadequacy of CIPN therapy is due to incomplete comprehension of the alterations triggered by the chemotherapeutic and affecting the excitability of peripheral sensory neurons, in which neuropathies are believed to arise. Identifying CIPN-specific disease pathways would dramatically improve our chances to develop specific pharmacological tools with higher efficacy and tolerability.

1.2. HCN channels in pain transmission

In the past decade, it has been demonstrated that HCN channels, mediating the Hyperpolarization-activated current (I_h), have a prominent role in controlling the excitability of nociceptive neurons and, therefore, in driving peripheral pain transmission (Momin et al., 2008; Emery et al., 2011; Young et al., 2014; Resta et al., 2016). In this respect, the efficacy of HCN blockers has been demonstrated in various neuropathic pain models (Dalle and Eisenach, 2005; Jiang et al., 2008; Takasu et al., 2010), suggesting a prominent role of these channels in maintaining chronic pain state. In 2011, Descoeur and collaborators reported an increase in HCN1 mRNA levels in DRG from oxaliplatin (OXA)-treated mice. They also demonstrated that ivabradine (IVA), a commercial HCN blocker (Berdeaux et al., 2009), reduces OXA-induced hyperalgesia and cold allodynia (Descoeur et al., 2011). Similar results were obtained by Young and collaborators (Young et al., 2014). Although strongly suggesting a prominent role for HCN channels in OXA-induced neuropathy, these studies lack to demonstrate the nature of the alterations undergone by HCN channels following chronic exposure to platinum compounds, i.e., whether a change in the expression pattern of HCN isoforms takes place, or, rather, their biophysical properties are affected. In a translation perspective, the anti-hyperalgesic potential of “pan” HCN blockers (i.e., not discriminating among HCN isoforms) cannot be fully exploited due to the detrimental effect that block of HCN4 in the sinus atrial node may have on cardiac rhythm (Novella Romanelli et al., 2016; Sartiani et al., 2017; Stillitano et al., 2013). In this work, we demonstrate that nociceptor neurons from OXA-treated rats show significant I_h gain of function in *ex vivo* recordings. Biochemically, we observed downregulation of HCN2 protein and upregulation of the HCN channels ancillary β -subunit Mink Related Peptide1 (MiRP1), known to increase the open probability of HCN1. In addition, we report the efficacy of the selective HCN1 inhibitor MEL57A in reducing hyperalgesia in CIPN-expressing rats without effects on cardiac rhythm. In conclusion, this study strengthens the evidence for a disease-specific role of HCN1 in CIPN, and proposes HCN1-selective inhibitors as new-generation pain medications with the desired efficacy and safety profile.

2. Methods

2.1. Animals

Two-month old male Wistar rats (Envigo, Varese, Italy), approximately 220–250 g at the beginning of the experimental procedure, were used for all experiments. Animals were housed at CeSAL (Centro Stabulazione Animali da Laboratorio, University of Florence) and used at least one week after their arrival. Four rats were housed per cage (size 26 × 41 cm) kept at 23 ± 1 °C with a 12-h light/dark cycle (light on at 7 a.m.). Animals were fed a standard laboratory diet and had access to tap water *ad libitum*. All animal manipulations were carried out according to the Directive 2010/63/

EU of the European parliament and of the European Union council (22 September 2010) on the protection of animals used for scientific purposes. The ethical policy of the University of Florence complies with the Guide for the Care and Use of Laboratory Animals of the US National Institutes of Health (NIH Publication No. 85-23, revised 1996; University of Florence assurance number: A5278-01). Formal approval to conduct the experiments described was obtained from the Animal Subjects Review Board of the University of Florence. Experiments involving animals have been reported according to ARRIVE guidelines (McGrath and Lilley, 2015). All efforts were made to minimize animal suffering and to reduce the number of animals used.

2.2. OXA neuropathic pain model

Rats were treated with OXA (2.4 mg/kg), administered intraperitoneally (i.p.) for 5 consecutive days every week for 2 weeks (10 i.p. injections) (Cavaletti et al., 2001). OXA was dissolved in 5% glucose solution. Control animals received an equivalent volume of 5% glucose i.p. (vehicle).

2.3. Administration of HCN blockers

4-Ethylphenylamino-1,2-dimethyl-6-methylaminopyrimidinium chloride (ZD7288) (1–10 mg/kg; Tocris) and IVA (0.1–5 mg/kg; Sigma-Aldrich) were dissolved in saline solution and administered i.p. and s.c., respectively. MEL57A (0.1–10 mg/kg) was suspended in 1% carboxymethylcellulose sodium salt (CMC) and p.o. administered. All acute treatments started 15 days from the beginning of OXA injections.

2.4. Paw pressure test

The nociceptive threshold was determined with an analgesimeter (Ugo Basile, Varese, Italy) as previously described (Di Cesare Mannelli et al., 2017). Briefly, a constantly increasing pressure was applied to a small area of the dorsal surface of the hind paw using a blunt conical mechanical probe. Mechanical pressure was increased until vocalization or a withdrawal reflex occurred while rats were lightly restrained. Thresholds were expressed in grams. Rats scoring below 40 g or over 75 g during the test before drug administration (25%) were rejected. An arbitrary cut-off value of 100 g was adopted. The data were collected by an observer who was blinded to the protocol.

2.5. von Frey test

The animals were placed in 20 × 20 cm Plexiglas boxes equipped with a metallic meshy floor, 20 cm above the bench. A habituation of 15 min was allowed before the test. An electronic von Frey hair unit (Ugo Basile, Varese, Italy) was used, and the withdrawal threshold was evaluated by applying force ranging from 0 to 50 g with a 0.2 g accuracy. Punctuate stimulus was delivered to the mid-plantar area of each anterior paw from below the meshy floor through a plastic tip and the withdrawal threshold was automatically displayed on the screen. Paw sensitivity threshold was defined as the minimum pressure required to elicit a robust and immediate withdrawal reflex of the paw. Voluntary movements associated with locomotion were not taken as a withdrawal response. Stimuli were applied on each anterior paw with an interval of 5 s. The measurement was repeated 5 times and the final value was obtained by averaging the 5 measurements (Sakurai et al., 2009).

2.6. Plantar test

The Hargreaves radiant heat method was carried out as demonstrated by (Tao et al., 2004). The rats were placed individually in clear plastic chambers of Ugo Basile plantar test apparatus for 20 min prior to the experiment for adaptation. Heat stimulation was applied at IR 60 (infrared intensity 50) on the paw with a 30-s cut-off time. The paw withdrawal latency comprised the time from the start of the beam light until the animal withdrew the paw from the heat stimulus (reaction time) was measured.

2.7. DRG neurons culture

Rat dorsal root ganglion (DRG) neurons were prepared as previously described (Vellani et al., 2004). Briefly, 20–30 ganglia were isolated, incubated in collagenase (2.5 mg ml⁻¹) for 1 hour at 37 °C and mechanically triturated with a 45 µm sterile needle. The cell suspension was filtered in 70 µm Nylon filter (BD Falcon) then centrifuged and re-suspended in Dulbecco's modified Eagle's medium (DMEM, Gibco) supplemented with 50 u ml⁻¹ penicillin and 0.05 mg/ml streptomycin (Invitrogen), 1% L-glutamine (Invitrogen), 10% fetal bovine serum (FBS, Gibco), 50 ng/ml nerve growth factor (NGF, Promega) and 1.25 µg/ml cytosine β-D-arabinofuranoside (Ara-C, Sigma). DRG neurons were plated onto 13 mm borosilicate cover glass previously coated with polyL-lysine (100 µg ml⁻¹, Sigma) and laminin (10 µg/ml, Sigma). The medium was changed after 24 h. All electrophysiology recordings were made within 48 h from dissociation. DRG neurons were classified based on diameter of somata as follows: small (<25 µm), medium (25–35 µm) and large (>35 µm).

2.8. Whole-cell patch clamp recordings

Voltage clamp experiments were performed using a PC-505B amplifier (Warner, Hamden, CT, USA) and digitalized with a Digidata 1440 A and Clampex 10 (Axon, Sunnyvale, CA, USA). Pipettes, resistance 3–4.5 MΩ, were pulled from borosilicate capillaries (Harvard Apparatus, London, UK) using a Narishige PP830 vertical puller (Narishige International Ltd, London, UK). Access resistance was monitored during whole-cell voltage clamp recordings throughout experiments with short, -10 mV steps. Recordings undergoing ≥10% drift in access resistance were discarded. Pipette capacitance transients were cancelled while no whole-cell compensation was used. Signals were sampled at 10 kHz, low-pass filtered at 1 kHz. All recordings were made at 21–22 °C. Ih was activated with a two-step protocol, consisting of a sequence of hyperpolarizing voltage steps (1 s) from -50 to -140 mV, followed by a step at -140 mV (holding potential -60 mV). Ih activation curves were obtained plotting the Ih tail currents against each imposed potential and were fitted with a Boltzmann equation of the following form:

$$I_t / I_t(\max) = 1 / 1 + \exp [(V_m - V_{1/2}) / k]$$

Where V_m is the membrane potential, $V_{1/2}$ is the membrane potential at which Ih is at half-maximal activation, k is the slope factor, I_t is the current amplitude of the tail current recorded for a given pre-pulse and $I_t(\max)$ is the maximum current amplitude of the tail current. Ih current rate of activation in small neurons we fit the current trace with a double exponential function the time constant (s) of Ih activation was determined by fitting currents with a double exponential function as described previously (Yao et al., 2003): $I_h(t) = A_f \exp(-t/\tau_f) + A_s \exp(-t/\tau_s)$. The activation curve was obtained from the tail current amplitude and the conductance (G) at each step voltage was normalized to the conductance

at -130 mV (G_{\max}) as previously reported (Cheng and Zhou, 2013). Extracellular solution contained (in mM): 140 NaCl, 2 CaCl₂, 1 MgCl₂, 3 KCl, 10 HEPES, 10 D (+) glucose, adjusted to pH 7.3 with NaOH, osmolarity 300–310 mosmol/l. Pipette were filled with an intracellular solution containing (in mM): 140 K + -gluconate, 10 HEPES, 5 EGTA, 2 MgCl₂, 5 Na₂Pcreatine, 0.3 NaGTP, 2 MgATP and adjusted to pH 7.3 with KOH, osmolarity 310–315 mosmol/l. Cells were continuously perfused with extracellular solution using gravity-fed perfusion system. All substances were dissolved in water to obtain 1000-fold stock solutions prior to use.

2.9. Western blot

Western blot (WB) analysis of DRGs was performed as previously reported (Laurino et al., 2015). Briefly, ganglia were isolated from the full length of the spinal column and homogenised in a buffer containing Tris HCl pH 8 50 mM, NaCl 150 mM, EDTA 1 mM, SDS 0.1% p/v and a Protease and Phosphatase Inhibitor Cocktail (Thermo Scientific, Monza, Italy). Proteins (20 µg) isolated from DRG were separated on 8% or 10% SDS-PAGE and transferred into PVDF membranes (60 min at 398 mA) using standard procedures. Blots were incubated overnight at 4 °C with specific antibody against HCN1, HCN2, HCN3, HCN4, KCNE2 (MiRP1) (Alomone Labs, Israel) and α-tubulin (clone DM1A, cn 05–829, Merck Millipore, Vimodrone, Milano) as reference protein. Primary antibodies were diluted in PBS containing 3% albumin and 0.05% Tween. The antigen-antibody complexes were visualized using appropriate secondary antibodies (1:10 000, diluted in PBS containing 3% albumin and 0.05% tween) and left for 1 hour at room temperature. Blots were then extensively washed and developed using an enhanced chemiluminescence detection system (Pierce, Rodano, Italy). Exposure and developing time were standardized for all blots. Densitometry of scanned images was performed on a Macintosh iMac computer using the public domain NIH Image program. Results represent mean ± SEM of three different gels and they are expressed as arbitrary units (AU), consisting of the ratio between the expression levels of the protein of interest and of α-tubulin.

2.10. Immunofluorescence

DRGs were isolated from the full length of the spinal column following removal of the spinal cord and fixed in 4% paraformaldehyde for 24 h and then cryo-embedded in Surgipath FSC22 (Leica Biosystems, USA). DRGs from 3 vehicle-treated and 3 OXA-treated rats were sectioned at 10 µm thickness and processed for immunofluorescence staining as previously described (Smith et al., 2015). Primary antibodies (Alomone Laboratories, Israel) were used as follows: HCN1, 1:1000; HCN2, 1:200; MiRP1, 1:50. Anti-rabbit Alexa Fluor 568 (1:400, Life Technologies) was used as a secondary antibody. Sections were counterstained with DAPI (Roche) and mounted in Prolong Gold (Life Technologies). All images were acquired with identical settings with a 20X objective (0.5NA, PL APO Fluotar), using a Leica DM6000B microscope equipped with a DFC350FX camera (Leica Microsystems). Image analysis was performed using Fiji-ImageJ (Schindelin et al., 2012) as follows: for each cell analysed the maximum diameter and the mean fluorescence intensity were measured. DRGs were then classified as small (diameter <25 µm), medium (diameter between 25 and 35 µm) and large (diameter >35 µm) and the mean fluorescence intensity in the 3 DRGs groups was statistically analysed by 2-way ANOVA with Bonferroni correction for multiple comparisons, using Graphpad Prism software.

2.11. Heart rate measurement

The frequency of the pulsations of caudal artery was determined daily in conscious restrained rats by tail-cuff plethysmography. The instrument used was a BP2000 blood pressure analysis system designed and built by John E. Rogers and James P. Rogers (Visitech Systems, Inc, Apex, NC). This system measures the heart rate, expressed as beats per minute (bpm), with the use of an optical sensor. Before the beginning of the experiments, rats were conditioned one week to the procedure and manipulation. After habituation to the tail cuff apparatus and stabilization of the heart rate, each group of animals (CTRL and OXA) were treated with oral administration of IVA (5 mg/kg) and MEL57A (30 mg/kg). Measurements were repeated at 30, 60, 120 and 180 min after IVA administration and at 15, 30, 45 and 60 min for MEL57A.

2.12. Data presentation and statistical analyses

Results are expressed as means \pm S.E.M. All datasets were tested for approximation to a normal distribution with a D'Agostino test (Graphpad Prism). Datasets were then analysed using parametric statistical tests, *t*-test for single comparisons or two-way analysis of variance [ANOVA] with Bonferroni post-hoc correction for multiple comparisons, and non-parametric Fisher exact test. Mean differences were considered significant for $p < .05$ (*); $p < .01$ (**); $p < .001$ (***). Data were analysed using Origin 9 software (OriginLab, Northampton, USA). Electrophysiological recordings, as well as WB panels and immunofluorescence microscopic images

shown in figures are intended to represent typical observations.

3. Results

3.1. *I_h* gain of function in DRG neurons from OXA-treated rats

We used standard patch clamp electrophysiology to characterize the properties of *I_h* current in dissociated DRG neurons from control (CTRL) and OXA-treated rats (OXA). We classified DRG neurons by cell body diameter as large ($>35 \mu\text{m}$), medium ($<35 \mu\text{m}$) and small ($<25 \mu\text{m}$), according to the literature (Harper and Lawson, 1985), and measured the capacitance, resistance and rheobase of the three categories. We observed that the passive membrane properties did not change following OXA treatment (SIA-B). The neuron-size classification allowed us to discriminate C and A δ nociceptive fibers, represented by small and medium size neurons, from non-nociceptive A β fibers represented by large neurons (Emery et al., 2011; Harper and Lawson, 1985; Momin et al., 2008). On these premises, we first studied the amplitude of *I_h* current in DRG neurons from CTRL and OXA groups. Results are schematized in Fig. 1, while complete numerical values are reported in Table 1. We found that *I_h* current density was significantly increased in small- and medium-size OXA neurons (Fig. 1A and B). In contrast, the difference in *I_h* current density between large-size (non-nociceptive) neurons from the two groups did not achieve statistical significance (Fig. 1B, bottom). These results indicate a sizeable gain of function of *I_h* in putative nociceptive neurons. A similar OXA-induced increase in *I_h* current density was also seen in

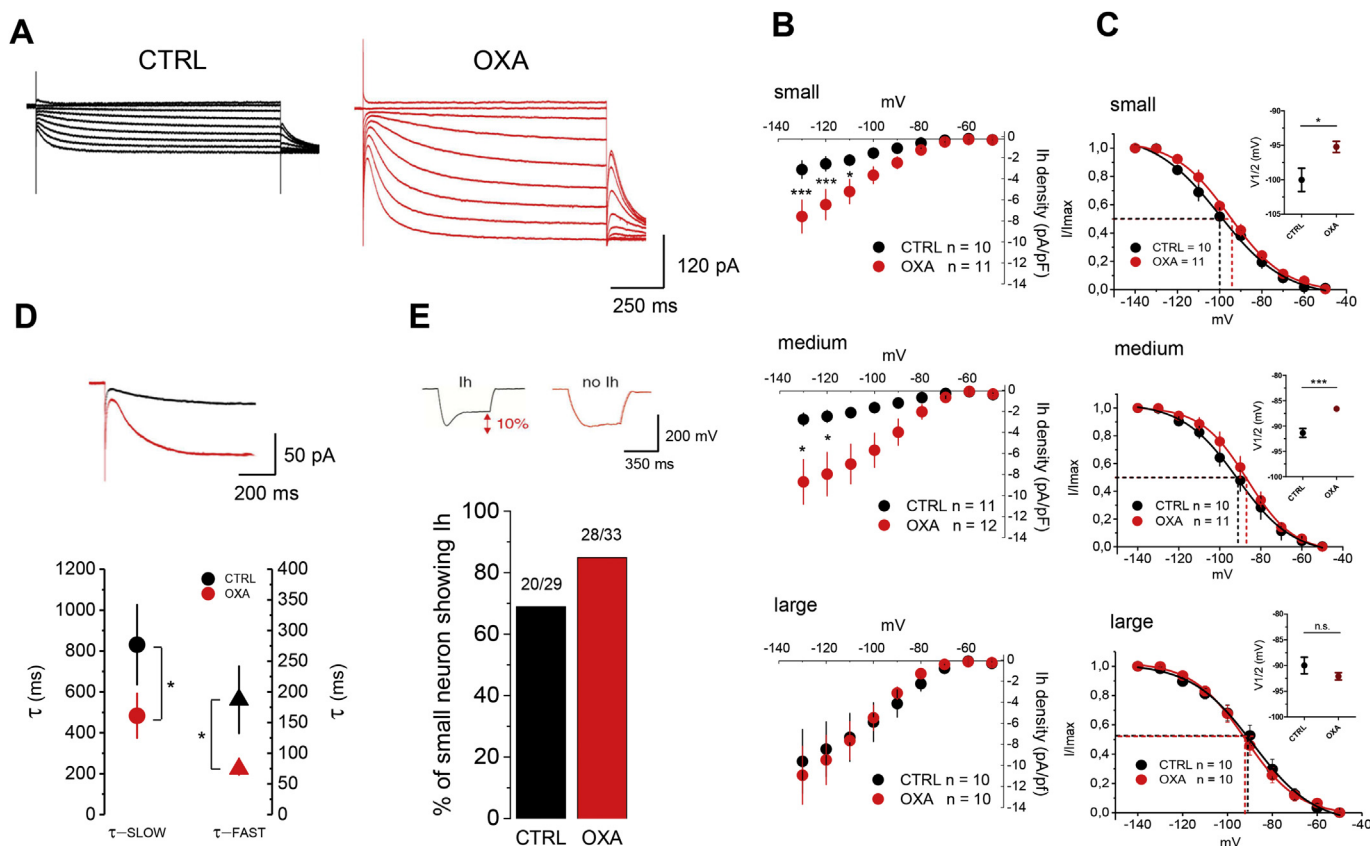


Fig. 1. *I_h* current gain of function in primary sensory neurons cultured from OXA-treated rats. **A.** *I_h* current traces in small neurons of dissociated DRGs from control (CTRL) and OXA-treated animals (OXA). **B.** Comparison of *I_h* current density among small, medium and large size DRG neurons of the two groups. **C.** Voltage dependence of *I_h* current in small, medium and large size DRG neurons. Inset, dot plot of *V_{1/2}* values in CTRL and OXA neurons. **D.** DRG neurons from CTRL and OXA animals have a comparable percentage of *I_h*-positive neurons, as assessed by determining the percentage of neurons expressing the typical "voltage sag" (top). **E.** Top, superimposed current traces obtained with a step to -90 mV in small neurons from CTRL and OXA neurons to highlight the different activation kinetics. Bottom, dot plot showing τ_{fast} and τ_{slow} of *I_h* activation (test step = -90 mV).

Table 1

Ih properties of small, medium and large neurons cultured in presence of NGF.

Neuron class	Ih properties	CTRL (n)	OXA (n)	p values – test (p)
Small	density (pA/pF)	-3.12 ± 0.63 (10)	-6.98 ± 1.20 (11)	2.5E-5 - 2 way ANOVA (6.2E-5)
	V1/2 (mV)	-100.02 ± 1.69 (10)	-95.22 ± 0.80 (11)	.024 - Unpaired <i>t</i> -test
Medium	density (pA/pF)	-2.77 ± 0.61 (11)	-8.70 ± 2.11 (12)	.021 - 2 way ANOVA (0.016)
	V1/2 (mV)	-91.36 ± 0.89 (10)	-86.60 ± 0.51 (11)	6E-4 - Unpaired <i>t</i> -test
Large	density (pA/pF)	-9.62 ± 3.03 (10)	-10.03 ± 1.95 (7)	.201 - 2 way ANOVA (0.20)
	V1/2 (mV)	-89.88 ± 1.10 (10)	-92.70 ± 0.50 (8)	.098 - Unpaired <i>t</i> -test

Results are expressed as means \pm S.E.M.Current density values are reported at the test step of -130 mV.**Table 2**

Ih properties of small, medium and large neurons cultured in absence of NGF.

Neuron class	Ih properties	CTRL (n)	OXA (n)	p values – test (p)
Small	density (pA/pF)	-3.34 ± 1.68 (10)	-7.75 ± 1.72 (11)	2.3 E-4 – 2 way ANOVA (9.2 E-4)
	V1/2 (mV)	-98.36 ± 2.60 (10)	-86.37 ± 2.27 (11)	3.2 E-5 - Unpaired <i>t</i> -test
Medium	density (pA/pF)	-2.52 ± 1.4 (10)	-8.23 ± 3.45 (10)	4.4 E-3 - 2 way ANOVA (0.004)
	V1/2 (mV)	-95.01 ± 1.96 (10)	-83.76 ± 0.55 (10)	8 E-4 - Unpaired <i>t</i> -test
Large	density (pA/pF)	-10.65 ± 4.69 (10)	-13.04 ± 4.92 (10)	.997 - 2 way ANOVA (0.965)
	V1/2 (mV)	-85.22 ± 1.00 (10)	-85.29 ± 0.5 (10)	.950 - Unpaired <i>t</i> -test

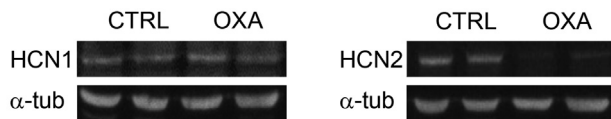
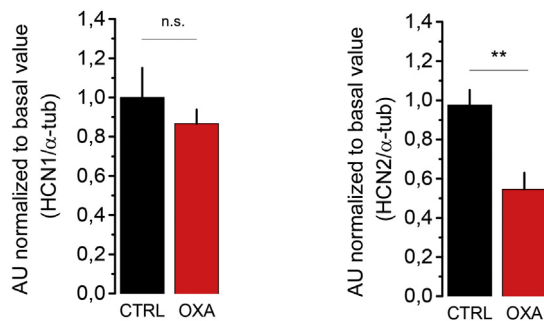
Results are expressed as means \pm S.E.M.Current density values are reported at the test step of -130 mV.**A****B**

Fig. 2. Expression of HCN subunits in intact DRGs from CTRL and OXA animals. **A.** WB experiment showing HCN1 (left), HCN2 (right) and respective α -tubulin signals. **B.** Densitometry of HCN1 (left) and HCN2 (right) protein levels expressed as HCN/ α -tubulin signal intensity. Bar graphs represents mean \pm SEM of 3 different experiments, $n = 6$ for each group.

a separate set of recordings from DRG neurons cultured in NGF-free medium (Table 2). We then tested the hypothesis that the biophysical properties of HCN channels were also altered in OXA neurons. To this end, we performed a standard two-step voltage clamp protocol and calculated activation curves from tail currents (DiFrancesco et al., 1986). The half-activation value ($V_{1/2}$) was extrapolated from activation curves and used to compare experimental groups. As shown in Fig. 1C, $V_{1/2}$ in small and medium-size neurons was significantly shifted towards depolarized potentials in the OXA group. Interestingly, only a non-significant trend to $V_{1/2}$ depolarization is seen in large neurons (1C, bottom). These results indicate a significant increase of the open probability of the HCN channels at physiological potential in nociceptive neurons caused

by *in vivo* OXA treatment. We then measured the activation kinetics of Ih in small neurons to uncover potential alterations in the biophysical properties of HCN channels. To this aim, we fitted current traces obtained at -90 mV with a double exponential function (see method), obtaining a fast and a slow time constant (τ_f , τ_s) near the $V_{1/2}$ potential (Fig. 1D). In agreement with the rightward shift in the activation curve, the kinetics of Ih activation was accelerated in OXA neurons (τ_f , CTRL, 187.3 ± 54.7 ms; OXA, 74.7 ± 10.1 ms; $n = 10$, $p < .05$. τ_s , CTRL, 831.1 ± 195.7 ms; OXA, 483.4 ± 108.9 ms; $n = 10$, $p < .05$). Moreover, we observed that there was no significant difference in the number of small DRG neurons showing Ih current, by estimating the percentage of neurons expressing a “voltage sag” equal to, or greater than 10% of the total voltage rebound elicited by a -200 pA hyperpolarizing current step (Emery et al., 2011). We recorded from 20/29 small CTRL neurons and 28/33 OXA neurons showing functional Ih ($p > .05$ Fisher's exact test, Fig. 1E). It was previously reported that Ih affects the resting membrane potentials (Biel et al., 2009; Dunlop et al., 2009; Pape, 1996). In our experimental paradigm, we observed a trend to depolarization of the RMP in OXA neurons (CTRL -52.12 ± 1.22 mV $n = 12$; OXA -48.72 ± 2.17 mV $n = 12$; $p > .05$). In summary, patch clamp analysis on dissociated DRG neurons indicates that small and medium neurons from OXA-treated animals show an electrophysiological profile dominated by a gain of function of Ih, which seems to depend on increased channel expression and/or altered biophysical properties.

3.2. OXA-induced neuropathy reduces HCN2 expression in DRG neurons

HCN1 and HCN2 are the most strongly expressed isoforms in DRG neurons (Emery et al., 2011; Momin et al., 2008). However, OXA-induced neuropathy might cause aberrant enhancement of HCN 3 and 4, which are normally poorly expressed in this tissue. Therefore, we performed Western Blot analysis of all isoforms with protein extracts from intact DRGs (Fig. 2A). We observed no significant alteration in the expression of HCN1 (CTRL, 1.01 ± 0.15 ; OXA, 0.86 ± 0.07 AU; $n = 6$; $p > .05$; Fig. 2A). Strikingly, HCN2 protein levels were reduced twofold in OXA rats compared to CTRL (CTRL, 0.97 ± 0.19 ; OXA, 0.54 ± 0.2 AU; $n = 6$; $p < .01$; Fig. 2B). HCN3

and 4 protein levels were very low in basal conditions showing either no change or even slightly reduced expression level, respectively (SII). In summary, WB analysis indicates that Ih gain of function does not depend on overall increased expression of HCN channels.

3.3. OXA-induced neuropathy increases the expression of MiRP1 in large, medium and small neurons

In the attempt to explain the paradoxical increase in Ih current density in the absence of an increase of HCN protein levels, we studied the expression of the ancillary subunit MiRP1, previously reported to boost HCN1 activation kinetics without affecting the protein expression (Brandt et al., 2009). Interestingly, we observed a significantly increased expression of MiRP1 in DRGs from OXA rats (CTRL, 0.96 ± 0.08 ; OXA, 1.26 ± 0.15 AU; $n = 6$; $p < .05$; Fig. 3A). In order to elucidate whether the elevation of MiRP1 expression was differential among distinct DRG neuron subsets, we performed immunofluorescence analysis on histological sections in intact DRGs from the two experimental groups (Fig. 3B). We observed that MiRP1 expression was increased of ~40% in all classes of DRG neurons (Fig. 3A and B bottom). This result is consistent with the increased current density and the enhanced gating kinetics that we observed in small and medium neurons from OXA-treated rats.

3.4. Anti-hyperalgesic efficacy of pan HCN blockers in an animal model of CIPN

Two weeks of chronic OXA administration (i.p., 2.4 mg/kg daily) in rats induces a progressive peripheral neuropathy recapitulating the peripheral painful state experienced by patients under OXA

chemotherapy, which is characterized by mechanical and thermal hypersensitivity. The entity of noxious and non-noxious mechanical stimulus transmission, as well as the hypersensitivity to noxious thermal stimuli characterizing OXA-induced peripheral neuropathy, were measured with the paw pressure, the von Frey test and the plantar test, respectively. On day 14, the weight tolerated on posterior paws by OXA animals (paw pressure test) decreased from 64.4 ± 1.6 g (vehicle + vehicle) to 42.9 ± 1.0 g (OXA + vehicle, $p < .01$ vs vehicle + vehicle) (Fig. 4B, top, left). Subcutaneous (s.c) injections of IVA at increasing doses (0.1–5 mg/kg), reduced mechanical hypersensitivity. Of note, the anti-hyperalgesic effect of IVA was dose dependent (Fig. 4B, bottom). The effect of 5 mg/kg IVA started 30 min after administration (56.4 ± 0.7 g) and peaked at 60 min (59.4 ± 0.6 g). The anti-hypersensitivity effect was still significant 120 min after treatment (50.5 ± 1.5 g, $p < .01$) vanishing at 180 min (45.0 ± 1.4 g). One mg/kg IVA showed the same long-lasting effect, with the strongest anti-hyperalgesic effect recorded 120 min after administration (56.4 ± 0.5 g, $p < .05$). The 0.1 mg/kg dose was ineffective (Fig. 4B top, left). In Fig. 4B, the withdrawal threshold to non-noxious mechanical stimulus is shown. von Frey test highlighted a decreased pain threshold at day 14 after OXA treatment (OXA + vehicle, 11.4 ± 0.3 g; vehicle + vehicle, 22.3 ± 0.6 g). Both 1 and 5 mg/kg IVA were able to significantly increase the withdrawal threshold of the animals starting 30 min after injection (19.6 ± 0.3 g, $p < .01$ and 17.0 ± 0.2 g, $p < .01$, respectively) and to reverse OXA-induced neuropathy after 60 min (23.7 ± 0.7 g, $p < .01$ and 22.1 ± 1.5 g, $p < .01$, respectively; Fig. 4B, top, middle). This effect lasted until 120 min after injection. IVA 0.1 mg/kg had no effect. Furthermore, acute IVA administration was able to counteract OXA-induced thermal hyperalgesia (plantar test). In this test, IVA (1–5 mg/kg) increased the licking latency in a

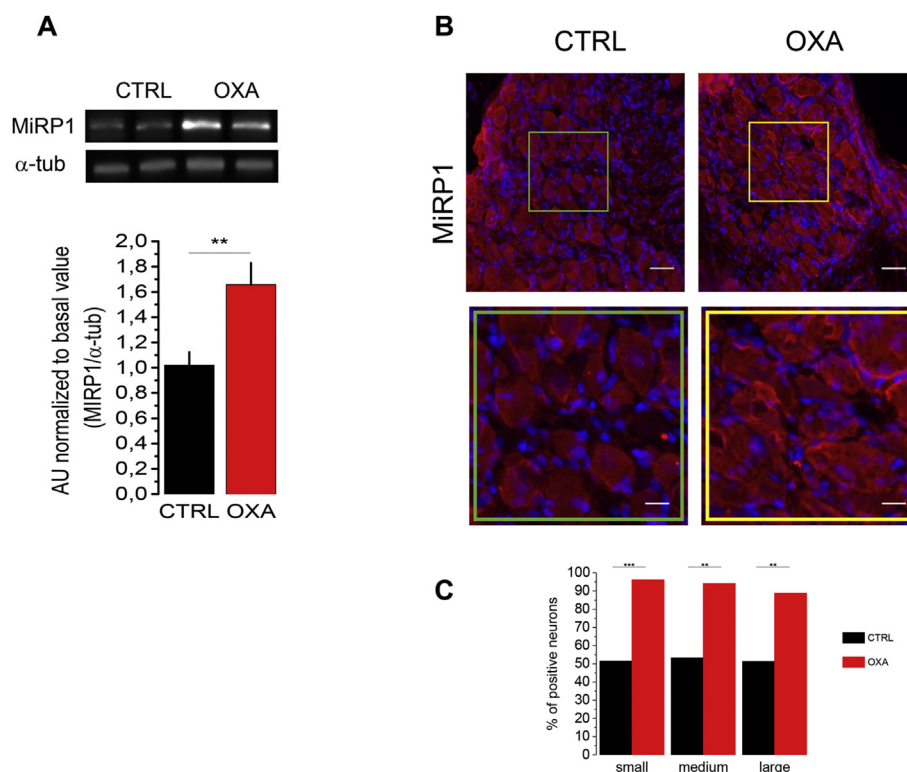


Fig. 3. Expression of MiRP1 subunit in intact DRGs from CTRL and OXA animals. **A.** Top, WB experiment showing MiRP1 and α -tubulin signals. Bottom, densitometry of MiRP1 protein levels expressed as MiRP1/ α -tubulin signal intensity. Bar graphs represent mean \pm SEM of 3 different experiments ($n = 6$ for each group). **B.** Top, Microphotographs of 10 μ m sections from intact CTRL (left) and OXA (right) DRGs immunostained for MiRP1 (red) and DAPI (blue; scale bar, 50 μ m). Bottom, magnifications of selected areas from CTRL (green box) and OXA (red box) DRGs (scale bar: 25 μ m). **C.** Number of positive/negative neurons represented as % of positive neuron in CTRL and OXA groups (statistical analysis: Fisher exact test). (For interpretation of the references to colour in this figure legend, the reader is referred to the Web version of this article.)

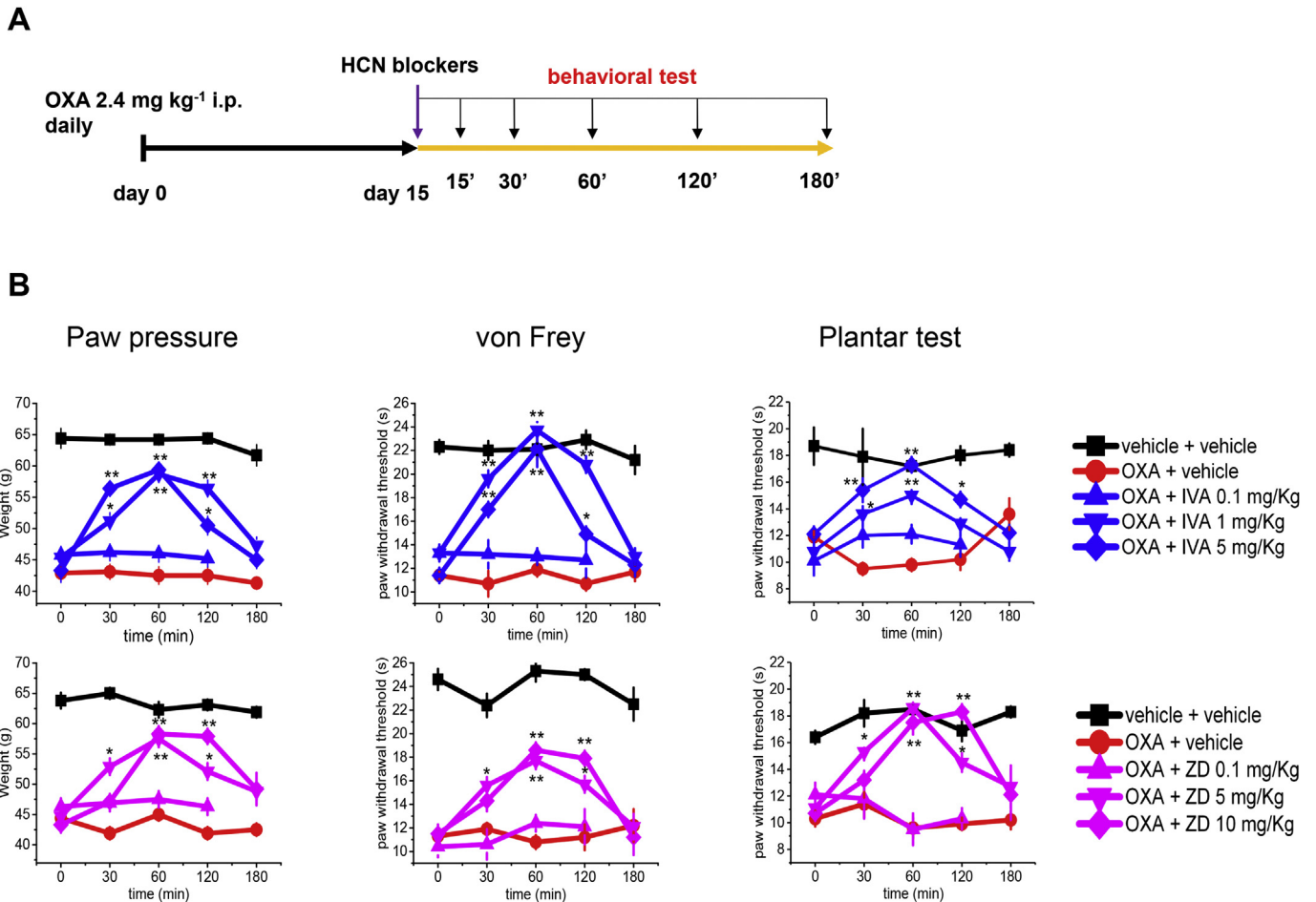


Fig. 4. Anti-hyperalgesic effects of pan HCN blockers. **A.** Schematic of *in vivo* experimental protocol. Animals were treated with increasing doses of ZD7288 (ZD) and IVA. Afterwards, animal behaviour was monitored for 180 min. **B.** Top, anti-hyperalgesic effects of ZD7288 in the paw pressure, von Frey and plantar tests. Bottom, anti-hyperalgesic effects of IVA in the paw pressure, von Frey and plantar tests.

dose-dependent manner with the highest efficacy reached by the 5 mg/kg dose (Fig. 4B top, right). The anti-hypersensitivity effect evoked by IVA treatment was significant from 30 until 120 min while the lower (0.1 mg/kg) dose was ineffective. IVA 5 mg/kg of administered in vehicle + vehicle group did not alter the pain threshold in control animals. For sake of comparison, we also tested the effect of another pan HCN blocker, ZD7288, which has been proved to exert anti-hypersensitivity effects in neuropathic pain models (Lee et al., 2005; Smith et al., 2015) (Fig. 4B, top). Acute i.p. treatment with the highest dose (10 mg/kg) reduced the mechanical hyperalgesia from 60 min after injection while the dose of 1 mg/kg induced a significant anti-hyperalgesic effect starting from 30 min. Both dosages were effective until 120 min after injection. The lower dose was ineffective at all time points (Fig. 4B, bottom, left). von Frey and plantar tests showed similar results (Fig. 4B bottom, middle and right). Moreover, ZD 10 mg/kg did not alter the nociceptive response in control animals.

3.5. Selective HCN1 block is sufficient to revert OXA-induced hyperalgesia

MEL57A is an IVA derivative recently developed by Romanelli and collaborators, with EC₅₀ = 0.32 ± 0.06 μM for HCN1 and 75.26 ± 14.38 μM for HCN4 in transfected HEK293 cells (Melchiorre et al., 2010; Del Lungo et al., 2012). We tested the efficacy of the compound on Ih current in OXA neurons, in which the HCN1 component is predominant. We observed that MEL57A (30 μM)

reduced Ih current amplitude by more than 50% in 10 min, the same time required by IVA and ZD7288 (Masi et al., 2015; Resta et al., 2016). As shown in Fig. 5B, normalized Ih conductance at -100 mV was significantly reduced in OXA neurons by MEL57A (CTRL, 0.67 ± 0.08; OXA, 0.33 ± 0.25; n = 5, p < .05). We then tested the ability of MEL57A to reduce hyperalgesia in neuropathic rats (Fig. 5C). MEL57A 1 mg/kg administered orally, significantly relieved mechanical hypersensitivity at 15 min (52.5 ± 1.2 g; p < .01). This effect peaked at 30 min (55.0 ± 0.9 g; p < .01) and vanished 45 min after treatment (47.9 ± 1.5 g). 10 mg/kg was able to reverse OXA neuropathy from 15 to 30 min after treatment (60.7 ± 1.3 g; p < .01 and 63.3 ± 0.8 g; p < .01, respectively). Anti-hyperalgesic efficacy was still significant at 45 min (52.4 ± 1.8 g; p < .01), while disappearing at 60 min (43.6 ± 1.5 g). The lower dose was ineffective (Fig. 5C left panel). Similar results were obtained with von Frey and plantar tests (Fig. 5C middle and right panels). In summary, administration of MEL57A was able to relieve both mechanical and thermal hypersensitivity induced by OXA in a dose dependent manner reverting the neuropathic symptoms from 30 to 45 min after the administration of the higher dose (Fig. 5C). 10 mg/kg MEL57A did not alter the nociceptive response in control animals.

3.6. MEL57A and IVA have similar anti-hyperalgesic efficacy, but MEL57A has no effects on heart rhythm

We assessed the anti-hyperalgesic efficacy of MEL57A relative to

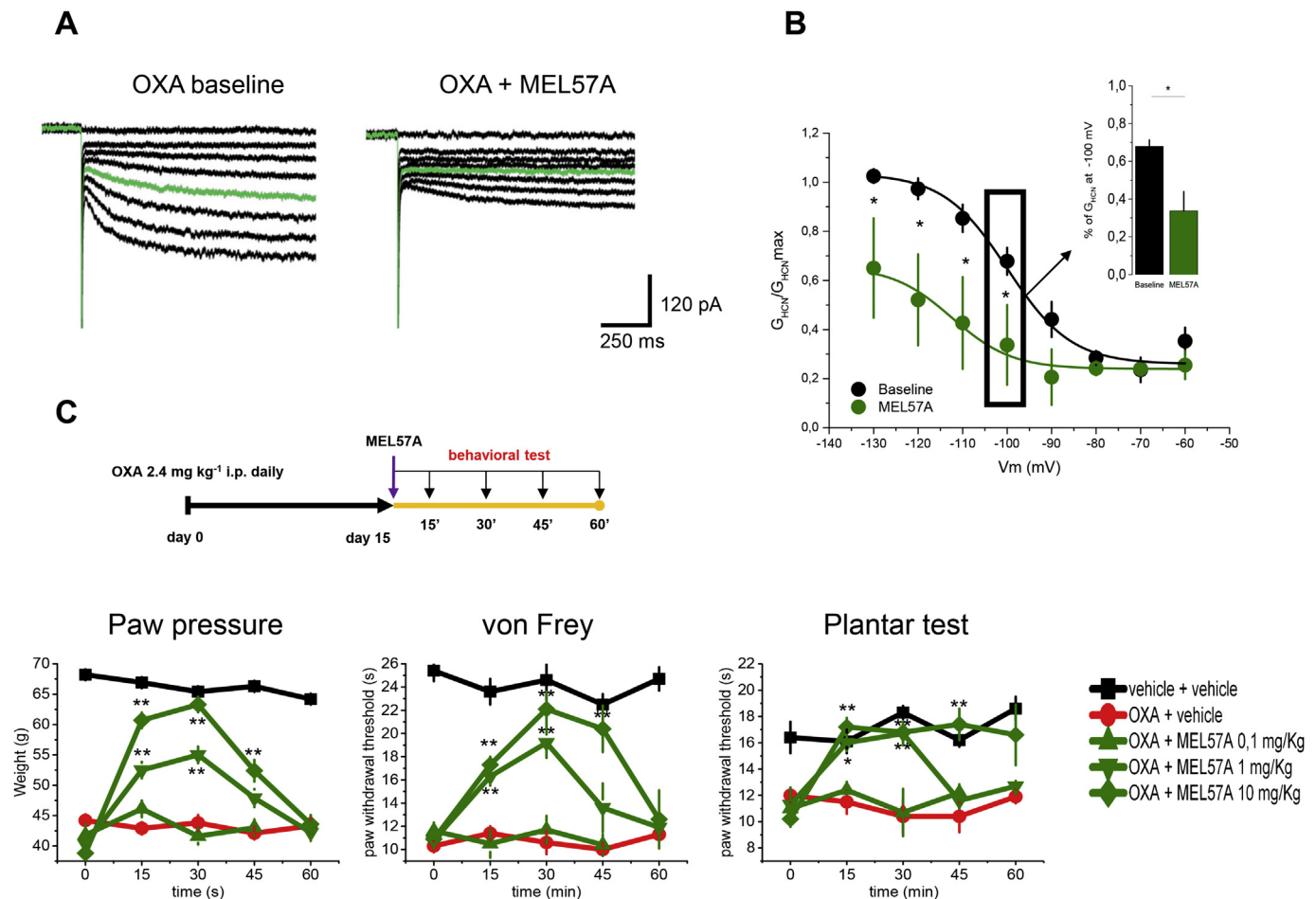


Fig. 5. Selective block of HCN1 by MEL57A reduced HCN channels conductance *in vitro* and induced anti-hyperalgesic effect *in vivo*. **A.** Ih current traces recorded in a small OXA neuron, before and 10 min after application of MEL57A. Green traces indicate the test step to -100 mV. **B.** Dot plot showing the effect of MEL57A on the HCN channels conductance. Inset, bar graph showing the percentage of open HCN channels at -100 mV. **C.** Top, schematic of *in vivo* experimental protocol. Bottom, anti-hyperalgesic effects of MEL57A in the paw pressure, von Frey and plantar tests. (For interpretation of the references to colour in this figure legend, the reader is referred to the Web version of this article.)

IVA by comparing the respective threshold values recorded in each test. We observed no significant differences in both the von Frey test (MEL57A, 22.1 ± 1.5 s; IVA, 23.7 ± 0.7 s; $p > .05$) and the plantar test (MEL57A, 16.8 ± 0.8 s; IVA, 17.3 ± 0.3 s; $p > .05$). Remarkably, MEL57A performed better than IVA in the paw pressure test (MEL57A, 63.3 ± 0.8 s; IVA, 59.4 ± 0.6 s; $p < .01$). These results suggest a similar anti-hyperalgesic efficacy reached by the selective block of HCN1, confirming the critical role of this HCN isoform in maintaining the peripheral neuropathy caused by OXA administration. A requirement for every drug designed to target Ih in peripheral neurons is to avoid or minimize the undesired effects resulting from inhibition of HCN isoforms expressed in the myocardium (Postea and Biel, 2011). CTRL and OXA rats received a single subcutaneous injection of MEL57A and IVA, each at the dose showing highest anti-hyperalgesic efficacy (10 and 5 mg/kg, respectively). As shown in Fig. 6, IVA significantly reduced the heart rhythm in both CTRL ($t_0 = 343 \pm 21$ bpm; $t_{60} = 273 \pm 11$ bpm; $n = 6$, $p < .01$, t_0 vs t_{60}) and OXA rats ($t_0 = 386 \pm 18$ bpm, $t_{60} = 307 \pm 14$ bpm; $n = 6$, $p < .05$, t_0 vs t_{60} ; $t_{120} = 293 \pm 25$ bpm; $n = 6$, $p < .01$, t_0 vs t_{120}). On the contrary, we did not observe changes in the heart rate following administration of the highest MEL57A dose in CTRL ($t_0 = 376 \pm 25$ bpm, $t_{60} = 368 \pm 16$ bpm; $n = 6$, $p > .05$; t_0 vs t_{60}) or in OXA rats ($t_0 = 370 \pm 26$ bpm, $t_{60} = 376 \pm 29$ bpm; $n = 6$, $p > .05$, t_0 vs t_{60}). These results confirm that MEL57A, at the dose showing the highest anti-hyperalgesic

efficacy in pain tests, does not block HCN channels in the SAN and thus does not alter the heart rate in either CTRL or OXA rats (Fig. 6).

4. Discussion

4.1. CIPN is accompanied by HCN1 gain of function

In this study we used an animal model of CIPN described by Cavaletti and collaborators in 2001 (Cavaletti et al., 2001). OXA administration at 2.4 mg/kg corresponds to the dosing employed in cancer patients (considering the Km factor 37 for the conversion of animal doses to the Human Equivalent Dose (Freireich et al., 1966; Reagan-Shaw et al., 2008)). The daily repeated administration of 2.4 mg/kg in the rat mimics the cumulative dosage of OXA eventually leading to chronic neuropathy in the clinical setting. (Cavaletti et al., 2001). By using patch clamp electrophysiology in dissociated DRG neurons from OXA rats we demonstrate that small and medium neurons show a gain of function of Ih. Increased current amplitude may result from increased channels expression on the cell surface or enhanced conductance due to modification in gating kinetics. By studying Ih voltage dependence, we observed a rightward shift in the $V_{1/2}$ as well as acceleration of activation kinetics in putative nociceptors. Therefore, we measured protein levels of all HCN isoforms by western blot and observed a decrease

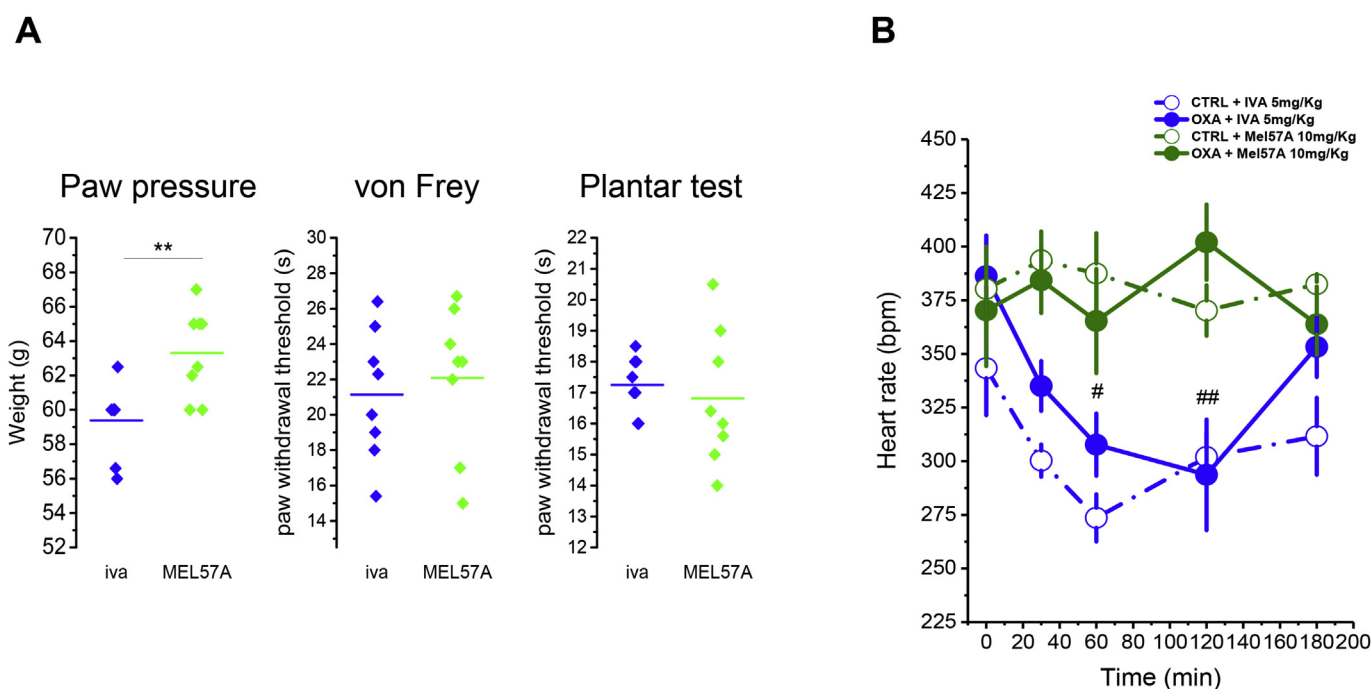


Fig. 6. Comparison between IVA (5 mg/kg) and MEL57A (10 mg/kg) for their anti-hyperalgesic efficacy and effect on the heart rate. **A.** Comparison of threshold values of IVA (60 min) and MEL57A (30 min) in the paw pressure, von Frey and plantar tests (scatter graph, raw data). **B.** Heart rate was recorded for 180 min following administrations of IVA or MEL57A in trained animals from both CTRL and OXA rats. A significant slowing of the heart rate was observed following administration of IVA in CTRL and OXA rats (blue circles). No significant alterations of the heart rate were observed following MEL57A administrations (green circles). Statistical comparisons are made between OXA + IVA and OXA + MEL57A. (For interpretation of the references to colour in this figure legend, the reader is referred to the Web version of this article.)

of HCN2 expression level in treated animals, in the absence of modifications of HCN1 protein levels. HCN 3 and 4 were nearly undetectable, as expected (Emery et al., 2011; Momin et al., 2008). These results are different from what observed by Descoeur et al. (2011). They found an increase in HCN1 mRNA without alteration of HCN2 mRNA, in DRG from mice treated with a single i.p. injections of OXA. In this regard, it must be noticed that our animal model is deeply different, consisting in a chronic treatment (15 days). Moreover, it is possible that HCN1 mRNA is upregulated while HCN1 protein is not, due to differential regulation at mRNA and protein synthesis levels. The observed reduction of HCN2 isoform could determine an increased HCN1/HCN2 ratio, thus a greater contribution of the HCN1-mediated component to global Ih current. This could explain the right shift in $V_{1/2}$ and the faster time constant of activation observed in medium and small-size neurons. In fact, HCN1 has the less negative $V_{1/2}$ and the fastest gating kinetics (Biel et al., 2009). To understand how Ih density and activation could be sped up without an increased expression of HCN channels, we measured the expression of the ion channel β -subunit MiRP1, which has been reported to increase the conductance and the activation kinetics of HCN channels (Abbott, 2012; Brandt et al., 2009; Yu et al., 2001). In agreement, with immunofluorescence on whole DRGs, we found elevated expression of MiRP1 in the DRG of OXA rats. Although not sufficient to establish a cause-effect link, the observed increase in MiRP1 expression may explain the OXA-induced pathological alteration of Ih function. Further studies will be needed to clarify the mechanisms linking HCN1-driven Ih gain of function to the alterations induced by chronic exposure to OXA.

4.2. Selective block of HCN1 reduces neuropathy without cardiac side effects

To study the role of the HCN gain of function on the expression

of neuropathy, we treated neuropathic animals with two different pan HCN blocker, IVA and ZD7288, and found that both induce a strong anti-hyperalgesic effect in mechanical and thermal pain tests confirming the critical role of the HCN channels in sustaining the transmission of neuropathic painful stimuli. However, to exploit the therapeutic potential of HCN channel blockers, one critical goal is to design isoform-specific compounds. New HCN channels-targeted analgesic compounds should feature sufficient selectivity for HCN1 or HCN2 over HCN4 channels expressed in pace-making cells of sinus atrial node, which play a major role during the diastolic depolarization phase of the heart rhythm. To this aim, we tested the HCN1-selective blocker MEL57A, recently developed by Romanelli and collaborators (Del Lungo et al., 2012; Melchiorre et al., 2010). After confirming the capability of MEL57A to reduce the HCN channels conductance in small DRG neurons, we tested it *in vivo* in increasing doses to study its potential anti-hyperalgesic effect. As expected, we observed that MEL57A induced anti-hyperalgesic effect with a potency and efficacy similar to IVA. Importantly, we compared the highest pain threshold of neuropathic animals following administration of IVA and MEL57A, observing no significant differences except for the paw pressure test, in which MEL57A seems to possess higher efficacy. Due to the reduction in HCN2 expression, combined to the overexpression of MiRP1, HCN1 component is expected to increase in OXA neurons. Thus, selective block of HCN1 is apparently sufficient to normalise pathological excitability of OXA-treated nociceptors, thus exerting an anti-hyperalgesic action, whose effectiveness matches that afforded by non-selective HCN blockers. The most important limitation to the use of IVA as an analgesic medication is the depressive effect on heart rate, which is undesirable in patients not suffering from angina (Postea and Biel, 2011). In order to study the effects of MEL57A on heart rhythm, we measured the heart rate of CTRL and OXA rats following acute

administration of IVA and MEL57A, and found that MEL57A is devoid of bradycardic action in both groups. This finding is of great relevance in view of the future clinical use of this one, or other HCN1 selective blockers. In summary, this work proposes a molecular mechanism explaining the paradoxical Ih gain of function, in the absence of overall HCN protein upregulation, characterizing neuropathic DRG neurons, and provides pharmacological evidence for a prominent role of HCN1 in CIPN. Importantly, the reported dysfunction of HCN1 channels is disease specific. This is a critical aspect towards the development of drugs with optimal efficacy and safety profile. Consistently, we found that selective HCN1 block has an effective and safe analgesic action in preclinical models of neuropathic pain. Interestingly, HCN1 gene expression increases in DRG neurons after paclitaxel treatment (Zhang and Dougherty, 2014), suggesting that Ih gain of function may be envisioned as a common pathogenic mechanism involved in the development of neuropathic states induced by different chemotherapeutics. To conclude, MEL57A, by selectively blocking HCN1 at peripheral level, could represent a promising lead compound to further develop a new generation of analgesic drugs to control different types of CIPN.

Acknowledgments

This work was supported by a grant from the Ente Cassa di Risparmio di Firenze (MANNECRF14; GM).

Appendix A. Supplementary data

Supplementary data related to this article can be found at <https://doi.org/10.1016/j.neuropharm.2018.01.014>.

References

- Abbott, G.W., 2012. KCNE2 and the K (+) channel: the tail wagging the dog. *Channels (Austin)* 6, 1–10.
- Addington, J., Freimer, M., 2016. Chemotherapy-induced peripheral neuropathy: an update on the current understanding. *F1000Res* 5.
- Avan, A., Postma, T.J., Ceresa, C., Cavaletti, G., Giovannetti, E., Peters, G.J., 2015. Platinum-induced neurotoxicity and preventive strategies: past, present, and future. *Oncologist* 20, 411–432.
- Berdeaux, A., Tissier, R., Couvreur, N., Salouage, I., Ghaleh, B., 2009. Heart rate reduction: beneficial effects in heart failure and post-infarcted myocardium. *Therapie* 64, 87–91.
- Biel, M., Wahl-Schott, C., Michalakakis, S., Zong, X., 2009. Hyperpolarization-activated cation channels: from genes to function. *Physiol. Rev.* 89, 847–885.
- Bokhari, F., Sawatzky, J.A., 2009. Chronic neuropathic pain in women after breast cancer treatment. *Pain Manag. Nurs.* 10, 197–205.
- Brandt, M.C., Endres-Becker, J., Zagidullin, N., Motloch, L.J., Er, F., Rottlaender, D., Michels, G., Herzig, S., Hoppe, U.C., 2009. Effects of KCNE2 on HCN isoforms: distinct modulation of membrane expression and single channel properties. *Am. J. Physiol. Heart Circ. Physiol.* 297, H355–H363.
- Cavaletti, G., 2014. Chemotherapy-induced peripheral neurotoxicity (CIPN): what we need and what we know. *J. Peripher. Nerv. Syst.* 19, 66–76.
- Cavaletti, G., Tredici, G., Petruccioli, M.G., Dondè, E., Tredici, P., Marmiroli, P., Minoia, C., Ronchi, A., Bayssas, M., Etienne, G.G., 2001. Effects of different schedules of OXA treatment on the peripheral nervous system of the rat. *Eur. J. Canc.* 37, 2457–2463.
- Cheng, Q., Zhou, Y., 2013. Novel role of KT5720 on regulating hyperpolarization-activated cyclic nucleotide-gated channel activity and dorsal root ganglion neuron excitability. *DNA Cell Biol.* 32, 320–328.
- Dalle, C., Eisenach, J.C., 2005. Peripheral block of the hyperpolarization-activated cation current (Ih) reduces mechanical allodynia in animal models of post-operative and neuropathic pain. *Reg. Anesth. Pain Med.* 30, 243–248.
- Del Lungo, M., Melchiorre, M., Guandalini, L., Sartiani, L., Mugelli, A., Koncz, I., Szel, T., Varro, A., Romanelli, M.N., Cerbai, E., 2012. Novel blockers of hyperpolarization-activated current with isoform selectivity in recombinant cells and native tissue. *Br. J. Pharmacol.* 166, 602–616.
- Descoeur, J., Pereira, V., Pizzoccaro, A., Francois, A., Ling, B., Maffre, V., Couette, B., Busserolles, J., Courteix, C., Noel, J., Lazdunski, M., Eschalier, A., Authier, N., Bourinet, E., 2011. OXA-induced cold hypersensitivity is due to remodelling of ion channel expression in nociceptors. *EMBO Mol. Med.* 3, 266–278.
- Di Cesare Mannelli, L., Pacini, A., Micheli, L., Femia, A.P., Maresca, M., Zanardelli, M., Vannacci, A., Gallo, E., Bilia, A.R., Caderni, G., Firenzuoli, F., Mugelli, A., Ghelardini, C., 2017. Astragali radix: could it be an adjuvant for OXA-induced neuropathy? *Sci. Rep.* 7, 42021.
- DiFrancesco, D., Ferroni, A., Mazzanti, M., Tromba, C., 1986. Properties of the hyperpolarizing-activated current (if) in cells isolated from the rabbit sinoatrial node. *J. Physiol.* 377, 61–88.
- Dunlop, J., Vasilyev, D., Lu, P., Cummons, T., Bowlby, M.R., 2009. Hyperpolarization-activated cyclic nucleotide-gated (HCN) channels and pain. *Curr. Pharmacol. Des.* 15, 1767–1772.
- Emery, E.C., Young, G.T., Berrococo, E.M., Chen, L., McNaughton, P.A., 2011. HCN2 ion channels play a central role in inflammatory and neuropathic pain. *Science* 333, 1462–1466.
- Freireich, E.J., Gehan, E.A., Rall, D.P., Schmidt, L.H., Skipper, H.E., 1966. Quantitative comparison of toxicity of anticancer agents in mouse, rat, hamster, dog, monkey, and man. *Cancer Chemother. Rep.* 50, 219–244.
- Harper, A.A., Lawson, S.N., 1985. Conduction velocity is related to morphological cell type in rat dorsal root ganglion neurones. *J. Physiol.* 359, 31–46.
- Jiang, Y.Q., Xing, G.G., Wang, S.L., Tu, H.Y., Chi, Y.N., Li, J., Liu, F.Y., Han, J.S., Wan, Y., 2008. Axonal accumulation of hyperpolarization-activated cyclic nucleotide-gated cation channels contributes to mechanical allodynia after peripheral nerve injury in rat. *Pain* 137, 495–506.
- Kim, J.H., Dougherty, P.M., Abdi, S., 2015. Basic science and clinical management of painful and non-painful chemotherapy-related neuropathy. *Gynecol. Oncol.* 136, 453–459.
- Laurino, A., De Siena, G., Resta, F., Masi, A., Musilli, C., Zucchi, R., Raimondi, L., 2015. 3-iodothyroacetic acid, a metabolite of thyroid hormone, induces itch and reduces threshold to noxious and to painful heat stimuli in mice. *Br. J. Pharmacol.* 172, 1859–1868.
- Lee, D.H., Chang, L., Sorkin, L.S., Chaplan, S.R., 2005. Hyperpolarization-activated, cation-nonspecific, cyclic nucleotide-modulated channel blockade alleviates mechanical allodynia and suppresses ectopic discharge in spinal nerve ligated rats. *J. Pain* 6, 417–424.
- Masi, A., Narducci, R., Resta, F., Carbone, C., Kobayashi, K., Mannaioni, G., 2015. Differential contribution of Ih to the integration of excitatory synaptic inputs in substantia nigra pars compacta and ventral tegmental area dopaminergic neurons. *Eur. J. Neurosci.* 42 (9), 2699–2706.
- McGrath, J.C., Lilley, E., 2015. Implementing guidelines on reporting research using animals (ARRIVE etc.): new requirements for publication in BJP. *Br. J. Pharmacol.* 172, 3189–3193.
- Melchiorre, M., Del Lungo, M., Guandalini, L., Martini, E., Dei, S., Manetti, D., Scapechi, S., Teodori, E., Sartiani, L., Mugelli, A., Cerbai, E., Romanelli, M.N., 2010. Design, synthesis, and preliminary biological evaluation of new isoform-selective f-current blockers. *J. Med. Chem.* 53, 6773–6777.
- Momin, A., Cadiou, H., Mason, A., McNaughton, P.A., 2008. Role of the hyperpolarization-activated current Ih in somatosensory neurons. *J. Physiol.* 586, 5911–5929.
- Novella Romanelli, M., Sartiani, L., Masi, A., Mannaioni, G., Manetti, D., Mugelli, A., Cerbai, E., 2016. HCN channels modulators: the need for selectivity. *Curr. Top. Med. Chem.* 16, 1764–1791.
- Pape, H.C., 1996. Queer current and pacemaker: the hyperpolarization-activated cation current in neurons. *Annu. Rev. Physiol.* 58, 299–327.
- Postea, O., Biel, M., 2011. Exploring HCN channels as novel drug targets. *Nat. Rev. Drug Discov.* 10, 903–914.
- Reagan-Shaw, S., Nihal, M., Ahmad, N., 2008. Dose translation from animal to human studies revisited. *Faseb. J.* 22, 659–661.
- Resta, F., Masi, A., Sili, M., Laurino, A., Moroni, F., Mannaioni, G., 2016. Kynurenine acid and zaprinast induce analgesia by modulating HCN channels through GPR35 activation. *Neuropharmacology* 108, 136–143.
- Roberts, J.A., Jenison, E.L., Kim, K., Clarke-Pearson, D., Langleben, A., 1997. A randomized, multicenter, double-blind, placebo-controlled, dose-finding study of ORG 2766 in the prevention or delay of cisplatin-induced neuropathies in women with ovarian cancer. *Gynecol. Oncol.* 67, 172–177.
- Sakurai, M., Egashira, N., Kawashiri, T., Yano, T., Ikeshue, H., Oishi, R., 2009. OXA-induced neuropathy in the rat: involvement of oxalate in cold hyperalgesia but not mechanical allodynia. *Pain* 147, 165–174.
- Sartiani, L., Mannaioni, G., Masi, A., Novella Romanelli, M., Cerbai, E., 2017. The hyperpolarization-activated cyclic nucleotide-gated: from biophysics to pharmacology of a unique family of ion channels. *Pharmacol. Rev.* 69, 354–395.
- Schindelin, J., Arganda-Carreras, I., Frise, E., Kaynig, V., Longair, M., Pietzsch, T., Preibisch, S., Rueden, C., Saalfeld, S., Schmid, B., Tinevez, J.Y., White, D.J., Hartenstein, V., Eliceiri, K., Tomancak, P., Cardona, A., 2012. Fiji: an open-source platform for biological-image analysis. *Nat. Med.* 9, 676–682.
- Smith, T., Al Otaibi, M., Sathish, J., Djouhri, L., 2015. Increased expression of HCN2 channel protein in L4 dorsal root ganglion neurons following axotomy of L5- and inflammation of L4-spinal nerves in rats. *Neuroscience* 295, 90–102.
- Stillitano, F., Lonardo, G., Giunti, G., Del Lungo, M., Coppini, R., Spinelli, V., Sartiani, L., Poggesi, C., Mugelli, A., Cerbai, E., 2013. Chronic atrial fibrillation alters the functional properties of if in the human atrium. *J. Cardiovasc. Electrophysiol.* 24, 1391–1400.
- Takasu, K., Ono, H., Tanabe, M., 2010. Spinal hyperpolarization-activated cyclic nucleotide-gated cation channels at primary afferent terminals contribute to chronic pain. *Pain* 151, 87–96.
- Tao, F., Tao, Y.X., Zhao, C., Doré, S., Liaw, W.J., Raja, S.N., Johns, R.A., 2004. Differential roles of neuronal and endothelial nitric oxide synthases during carrageenan-induced inflammatory hyperalgesia. *Neuroscience* 128, 421–430.
- Vellani, V., Zachrisson, O., McNaughton, P.A., 2004. Functional bradykinin B1

- receptors are expressed in nociceptive neurones and are upregulated by the neurotrophin GDNF. *J. Physiol.* 560, 391–401.
- Yao, H., Donnelly, D.F., Ma, C., LaMotte, R.H., 2003. Upregulation of the hyperpolarization-activated cation current after chronic compression of the dorsal root ganglion. *J. Neurosci.* 23, 2069–2074.
- Young, G.T., Emery, E.C., Mooney, E.R., Tsantoulas, C., McNaughton, P.A., 2014. Inflammatory and neuropathic pain are rapidly suppressed by peripheral block of hyperpolarisation-activated cyclic nucleotide-gated ion channels. *Pain* 155, 1708–1719.
- Yu, H., Wu, J., Potapova, I., Wymore, R.T., Holmes, B., Zuckerman, J., Pan, Z., Wang, H., Shi, W., Robinson, R.B., El-Maghrabi, M.R., Benjamin, W., Dixon, J., McKinnon, D., Cohen, I.S., Wymore, R., 2001. MinK-related peptide 1: a beta subunit for the HCN ion channel subunit family enhances expression and speeds activation. *Circ. Res.* 88, E84–E87.
- Zhang, H., Dougherty, P.M., 2014. Enhanced excitability of primary sensory neurons and altered gene expression of neuronal ion channels in dorsal root ganglion in paclitaxel-induced peripheral neuropathy. *Anesthesiology* 120, 1463–1475.